Criteria to observe single-shot all-optical switching in Gd-based ferrimagnetic alloys

Wei Zhang [1,2,3] Julius Hohlfeld,[3] Tian Xun Huang,[3] Jun Xiao Lin [3] Michel Hehn,[3] Yann Le Guen,[3] Jude Compton-Stewart,[3] Gregory Malinowski,[3] Wei Sheng Zhao,[1,2,*] and Stéphane Mangin[3,†]

[1]*International Innovation Institute, Beihang University, Hangzhou, China*
[2]*Fert Beijing Institute, BDBC, Beihang University, Beijing 100191, China*
[3]*Université de Lorraine, CNRS, IJL, F-54000 Nancy, France*

Single-shot all-optical helicity-independent switching (AO-HIS) induced by a femtosecond laser pulse has been mainly reported in gadolinium-based rare-earth (RE)–transition-metal alloys such as GdFeCo or GdCo, but the mechanism leading to magnetization switching is a hotly debated topic. Here, we elaborate on a large number of $Gd_y RE_{1-x-y} Co_x$ (RE = Dy, Tb, Ho) alloys to tune various magnetic parameters in order to define what the criteria are for observing AO-HIS in such systems. The state diagrams show that two laser-fluence thresholds must be considered: the fluence which induces the single laser-pulse switching (F_{switch}) and the fluence at which the material breaks into a multidomain state (F_{multi}). Those two fluences are shown to behave very differently as a function of the material properties and the laser-pulse duration. The criterion to ensure the observation of AO-HIS is $F_{multi} > F_{switch}$. Taking into account the parameters defining the conditions for which multidomain states are created and considering only the angular momentum transfer from the Gd sublattice to the rest of the system explains in large our experimental results. The importance of the compensation in the ferrimagnetic alloys is also discussed. We believe the defined criteria will be an important tool for designing ultrafast spintronic devices based on all-optical switching.

I. INTRODUCTION

As a powerful way to sense, store, and process digital information, magnetics-based technologies [1–3] undoubtedly promote the development of modern society. Controlling and manipulating magnetic configurations with simultaneously higher-energy efficiencies and at shorter timescales is not only a new challenge, but also an urgent issue for evolving information technology [4,5]. As the fastest external stimulus, the use of light is a promising approach to enhance the speed of data processing. As a prominent technique of light-induced magnetic manipulation, single-shot ultrafast all-optical helicity-independent switching (AO-HIS) [6] is of crucial importance for generating smaller, faster, and more energy-efficient information technology. AO-HIS taking place on a picosecond timescale has been demonstrated experimentally in a rather limited number of materials. It was first observed in gadolinium–transition-metal (Gd-TM) alloys (GdFeCo or GdCo) using a femtosecond laser pulse without any applied magnetic field [7–11]. In those heavy rare-earth–transition-metal (RE-TM) ferrimagnetic alloys, the magnetization of the TM sublattice is antiferromagnetically exchange coupled to the magnetization of the RE. Consequently, at certain compositions, a compensation temperature exists at which the net magnetization of the alloy is zero. Recently, breakthrough experiments have shown that single

laser-pulse switching can be achieved in multilayer structures including Gd/Co [12], Tb/Co [13] synthetic ferrimagnets, or the rare-earth-free Heusler alloy $Mn_2 Ru_x Ga$ [14]. Note that single-pulse switching in Tb/Co presents a very different switching mechanism, which is not ultrafast and shows a very different state diagram [15].

Single-pulse, ultrafast AO-HIS has been observed only in alloys and multilayers where two magnetization sublattices are antiferromagnetically coupled. Furthermore, with the known exception of $Mn_2 Ru_x Ga$ [14], the presence of gadolinium and an alloy concentration close to compensation is required. Indeed, in case of GdFeCo or GdCo alloys, several experimental and theoretical works have demonstrated that AO-HIS was possible only for a limited composition range around the compensation point [6,9,16–18]. Note that AO-HIS for TbCo alloys was predicted but has never been demonstrated [19]. This limits the range of materials which can be used for possible all-optical data storage applications. Moreover, it is still not clear (i) if we can reduce or remove Gd in the RE-TM alloys and still observe AO-HIS and (ii) if being close to compensation is the main material criterion for observing AO-HIS as suggested by the theories [6,18], or if other criteria must be met?

Fortunately, exploring the parameter spaces, such as material properties and laser-pulse characteristics (fluences F and pulse durations τ) for the observation of AO-HIS, is helpful to determine the criteria to be fulfilled to observe ultrafast, single-pulse AO-HIS. The effect of the above parameters on AO-HIS are summarized by building state diagrams showing the final magnetic state of the sample after a single laser

*weisheng.zhao@buaa.edu.cn
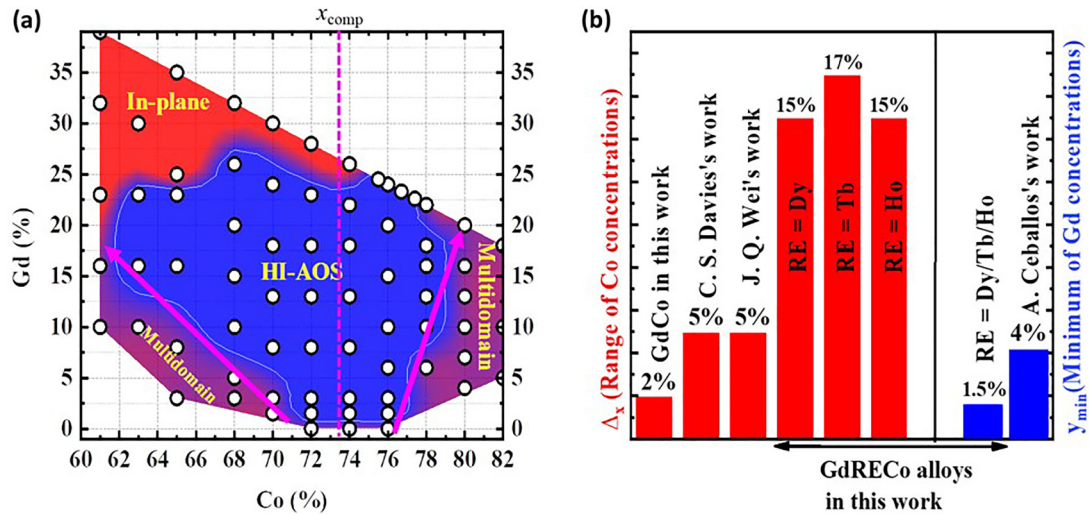†stephane.mangin@univ-lorraine.fr

094412-1

FIG. 1. (a) Mapping of the magnetic states after one single ultrashort laser pulse with 50-fs duration as a function of the Gd and the Co concentration for 10-nm-thick $Gd_y RE_{1-x-y}Co_x$ samples with $RE = Dy$. Depending on the concentrations, three regions can be defined as *in plane*, *AO-HIS*, and *multidomain states*. The vertical pink dashed line represents the compensation concentration. The two solid arrows are a guide to the eyes between AO-HIS and multidomain states. (b) Summary of the Co composition range (Δx) and minimum Gd compositions needed to observe single short laser pulse AO-HIS for various studies (Davies [9], Wei [16], and Ceballos [24]).

pulse as a function of F and τ. As described by Wei *et al.* [16], the state diagram for AO-HIS is shown to have a triangular shape, and three quantities corresponding to the three edges of this triangle can be determined and discussed. F_{switch}^{min} is the minimum fluence at which AO-HIS can be observed (usually for the shortest pulse duration), F_{multi} is the fluence defining the transition from AO-HIS to a multidomain state (almost independent of the pulse duration), and τ_{max} is the maximum pulse duration for which AO-HIS can be observed. Gorchon *et al.* [20] demonstrated that τ_{max} can be as long as 15 ps in GdFeCo. This challenged the accepted driving mechanism, being the ultrafast angular momentum transfer between RE and TM sublattices, since the initial experiments for AO-HIS used ultrashort ($\sim$100-fs-long) optical pulses. Later, Davies *et al.* [9], by modeling the ferrimagnet as two coupled macrospins, and Jakobs *et al.* [6] using an atomistic spin dynamics model, were able to reproduce that a large τ_{max} works for AO-HIS only if the alloy composition is close to compensation. However, all those studies have only been carried out for GdFeCo alloys, leaving the development of the state diagrams of other GdRECo alloys, such as $RE = Dy$, Tb, Ho, largely undocumented. This has also significantly limited our ability to establish a full criterion for AO-HIS observation.

In this work, we have grown series of 10-nm-thick $Gd_y RE_{1-x-y}Co_x$ thin-film alloys ($RE = Dy$, Tb, Ho) in order to determine the influence of composition on AO-HIS. We could first demonstrate AO-HIS for a much larger range of Co and RE concentrations than those seen in pure GdCo or GdFeCo alloys. The possibility to introduce rare earth such as Dy, Tb, and Ho in the alloys allows to increase the magnetocrystalline anisotropy and consequently increase the thermal stability of potential devices. Moreover, the amount of Gd needed to observe AO-HIS could be as low as 1.5%. We demonstrate that the characteristic F_{switch} versus τ and F_{multi} versus τ extracted from triangular state diagrams for AO-HIS vary differently with the alloy's magnetic parameters

such as M_s (saturated magnetization), J_{eff} (effective exchange coupling), K_u (magnetocrystalline anisotropy constant), and the amount of Gd. We could then define the criteria needed to be fulfilled to observe AO-HIS. We could demonstrate why in many cases being close to compensation is essential to observe magnetization switching under a single femtosecond laser.

II. EXPERIMENTAL RESULTS

Figure 1(a) shows the whole series of $Gd_y Dy_{1-x-y}Co_x$ alloys we studied in this work, with x varying between 61 and 80%. In this work, we mainly focus on the samples with perpendicular magnetic anisotropy (PMA) as our experimental optical setup allows the measurement of the out-of-plane magnetization component. Among the samples with PMA, two kinds of magnetic states can be distinguished after excitation by a single femtosecond laser pulse, i.e., the multidomain state represented by the dark-red region, and the deterministically switched state in blue marked within the white line. Note that for a few Gd-rich samples located in the red region, the magnetization is in plane, the orientation of which our experimental setup does not allow us to observe. For all the $Gd_y Dy_{1-x-y}Co_x$ and $Gd_y Ho_{1-x-y}Co_x$ alloys samples, a very similar mapping is observed, as shown in Figs. S1(a) and S1(b) in Note 1 of the Supplemental Material [21]. For $Gd_y Dy_{1-x-y}Co_x$ alloys, the concentration of Co (x) and Gd (y) allowing AO-HIS covers from $x = 63\%$ to $x = 78\%$, and $y = 1.5\%$ to $y = 26\%$. The engineering of RE-TM alloys with a large enough compositional window showing AO-HIS is highly desirable since the magnetic properties (M_s, K_u, T_c) can then be selected more decisively [22,23]. In Fig. 1(b), we summarized the range of Co compositions, and the minimum Gd compositions needed to show AO-HIS. By introducing other rare-earth elements Tb/Dy/Ho, the windows of Co concentrations (Δx) showing AO-HIS is $\Delta x = 17\%/15\%/15\%$,
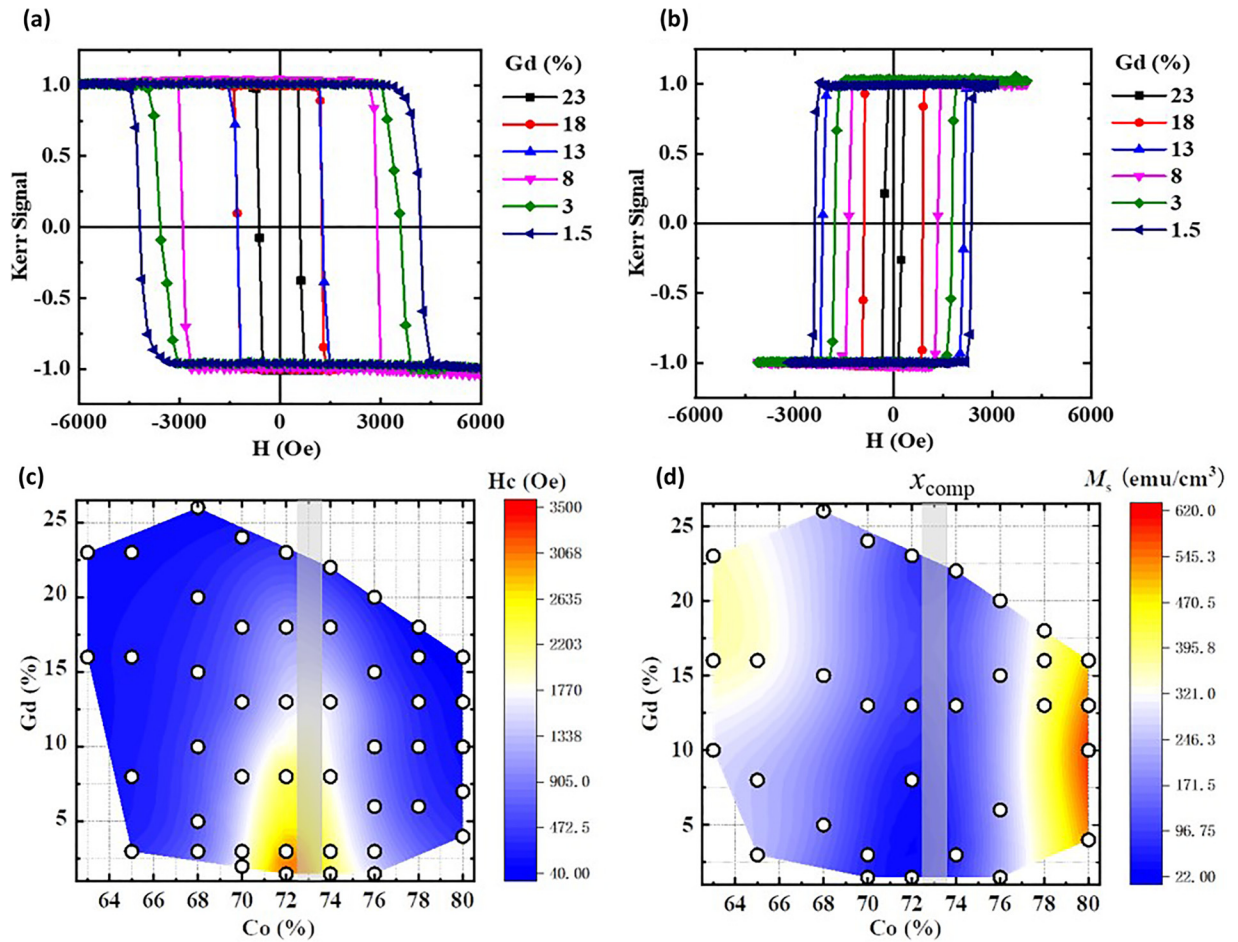
FIG. 2. Static magnetic properties of 10-nm $Gd_yDy_{1-x-y}Co_x$ films. (a), (b) Normalized magneto-optical Kerr effect (MOKE) as a function of the magnetic field H applied perpendicular to the film plane, with $x = 72$ and 74%, respectively. The hysteresis loops are inverted for (a) and (b), demonstrating that the magnetization compensation is obtained for a Co concentration between 72 and 74% for all Gd concentration. (c), (d) Mapping of the coercivity and the saturated magnetization as a function of Gd and Co concentration. Dots indicate measured data.

respectively, which is much larger than that for pure GdCo alloys (2%), and even larger than that in GdFeCo alloys (5%) reported by Wei [16] and Davies *et al.* [9]. Moreover, we found that a minimum Gd composition around 1.5% is enough to sustain the AO-HIS in $Gd_yRE_{1-x-y}Co_x$ alloys, a value lower than the results in GdTbCo alloys reported previously by Ceballos *et al.* [24].

A. Samples' magnetic properties

The magnetization of the samples, namely glass/Ta(5 nm)/Pt(3 nm)/$Gd_yRE_{1-x-y}Co_x$ (10 nm)/Pt(5 nm) has been measured by applying a field perpendicular to the film plane to determine if the sample magnetization is in plane or out of plane [Fig. 1(a)]. Figure 2(a) shows the hysteresis loops obtained using the magneto-optic Kerr effect (MOKE) at room temperature with a magnetic field applied perpendicular to the film plane for various $Gd_yDy_{1-x-y}Co_x$ alloys when $x = 72\%$. These square loops with 100% of remanence indicate a well-defined strong PMA of the samples. As compared with that for $x = 72\%$ in Fig. 2(a), the polarity of the hysteresis loops in Fig. 2(b) shows a reversed sign at concentration value of $x = 74\%$. Given that the MOKE technique senses

predominantly the Co subnetwork, the change of the signal's polarity suggests the magnetization compensation point x_{comp} is between $x = 72$ and 74% at room temperature, whatever the Gd concentration. This is consistent with the results in Fig. 1(a), where the boundary between Co-dominant and RE-dominant samples is around $x = 72\%$. Usually, the net magnetization approaches zero and the coercivity diverges at the magnetization compensation point [25]. In Figs. 2(c) and 2(d), a color scale from red to blue allows us to map the evolution of the coercivity (H_c) and saturation magnetization (M_s) as a function of the Co and Gd concentration in $Gd_yDy_{1-x-y}Co_x$. This demonstrates that the magnetic properties can be strongly affected by compositional changes. Obviously, the maximum coercivity and minimum saturation magnetization of $Gd_yDy_{1-x-y}Co_x$ occurs around $x = 72\%$, simultaneously. The presence of a shaded region highlights the compensation concentrations in these alloys in Figs. 2(c) and 2(d). Very similar behavior is observed for Tb- and Ho-based $Gd_yRE_{1-x-y}Co_x$ alloys. Even though the magnetization of those alloys reaches zero between $x = 72$ and 74%, the coercivity increases by replacing the Gd with one of the other rare earths. This is certainly due to the fact that the magnetocrystalline anisotropy K_u is higher when Gd (an S
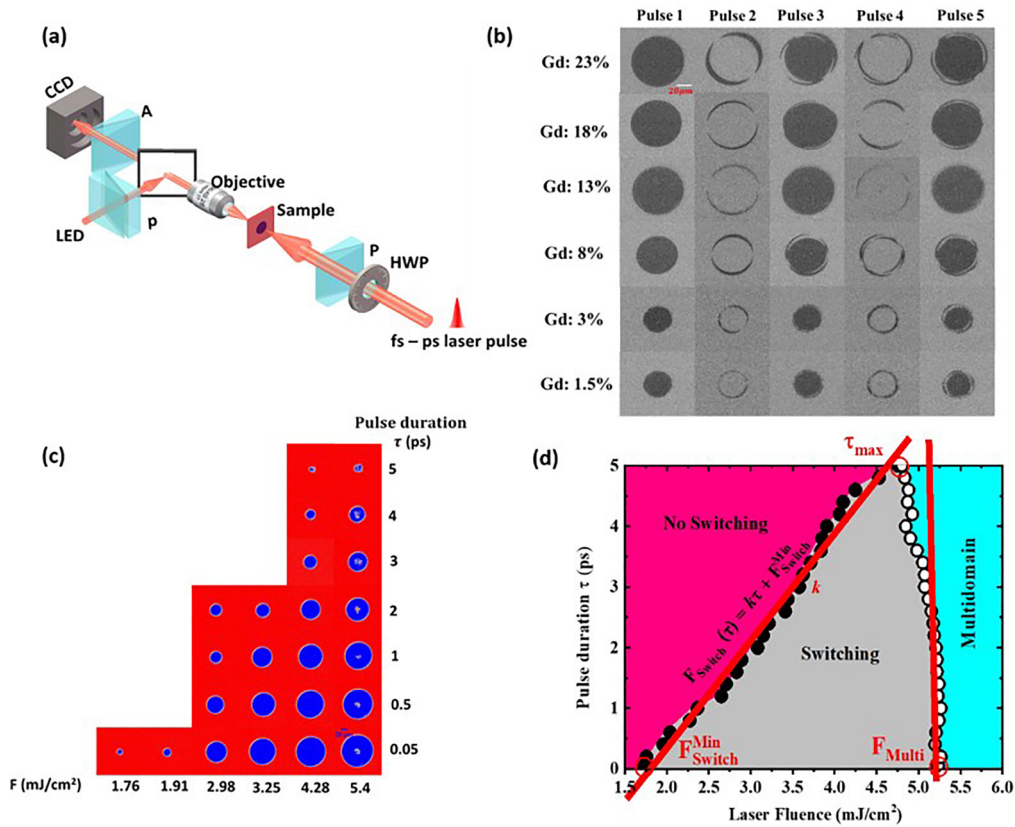
FIG. 3. Single-pulse all-optical magnetization toggle switching and construction of AO-HIS state diagrams. (a) Sketch of the MOKE microscopy setup using single femtosecond laser-pulse excitations. HWP: half wave plate; P: polarizer; A: analyzer; LED: light-emitting diode; CCD: charge-coupled device. (b) Magneto-optical images of 10-nm $Gd_yDy_{1-x-y}Co_x$ alloys with $x = 72\%$ and y varying from 1.5 to 23% after exposure to a sequence of single linearly polarized laser pulses with a pulse duration of $\tau = 50$ fs and a fluence $F = 3.2 \text{mJ/cm}^2$. (c) Magneto-optical images of 10-nm $Gd_yDy_{1-x-y}Co_x$ alloys with $x = 72\%$, $y = 23\%$, after exposure to a single linearly polarized laser pulse with various pulse durations (τ) and laser fluences (F). (d) Details of the state diagram constructed for $Gd_{23}Dy_5Co_{72}$: switching fluence F_{switch} (solid black dot) and multidomain fluence F_{multi} (open black dot) as a function of the pulse durations (τ). Three regions are defined by the evolution of $F_{\text{switch}}(\tau)$ and $F_{\text{multi}}(\tau)$: switching, no switching, and multidomain states. $F_{\text{switch}}^{\text{min}}$, k, and τ_{max} are defined by assuming $F_{\text{switch}}(\tau) = k\tau + F_{\text{switch}}^{\text{min}}$ and $F_{\text{switch}}(\tau_{\text{max}}) = F_{\text{multi}}(\tau_{\text{max}})$.

ion) is replaced by another RE (Tb, Dy, or Ho). In those $Gd_yRE_{1-x-y}Co_x$ alloys, the Curie temperature, T_c, and consequently the effective exchange coupling J_{eff}, increases when the Co concentration increases [22,23]. Furthermore, for a constant Co concentration, T_c will be higher for GdCo alloys than for TbCo alloys, which will in turn have higher T_c s than DyCo alloys and so on for HoCo alloys. In conclusion, with the three-sample series of $Gd_yTb_{1-x-y}Co_x$, $Gd_yDy_{1-x-y}Co_x$, and $Gd_yHo_{1-x-y}Co_x$ alloys we will be able to tune parameters such as M_s, T_c, J_{eff}, and K_u, and study their effect on the observed AO-HIS behaviors.

B. Single-shot AO-HIS in $Gd_yRE_{1-x-y}Co_x$ alloys

The experimental setup used to study single-shot AO-HIS is sketched in Fig. 3(a). Pictures are taken before and after each laser shot, to allow for a background image correction. The contrast is given by the magnetization projection along the direction perpendicular to the film plane. To ensure a well-defined initial state, the film is saturated using an external field whose exact value depends on the coercivity of the samples. We estimate that the picture is taken 1 s after the laser pulse.

In Figs. 3(b)–3(d), we focus on GdDyCo samples near the compensation point (x_{comp}), i.e., $Gd_yDy_{1-x-y}Co_x$, with $x = 72\%$, while y varies from 1.5 to 23%. A toggle-magnetization switching similar to the one observed for GdCo alloys is shown in Fig. 3(b) after five subsequent laser pulses with laser fluence $F = 3.2$ mJ/cm^2. Interestingly, deterministic reversal is achieved, even when the Gd concentration is as low as 1.5% (as much as 26.5% of Dy). The same result is obtained for Tb and Ho as shown in Fig. S2, where similar toggle-magnetization switching is also recorded for both GdTbCo$_{74}$ and GdHoCo$_{72}$ alloys. Here, the maximum concentrations of Tb (24.5%), Dy (26.5%), and Ho (26.5%) allowing for AO-HIS in Gd*RE*Co alloys are higher than the previously reported value of 18% for Gd$_4$Tb$_{18}$Co$_{78}$ [24]. As one can see from Fig. 1(a), the minimum value of y (Gd concentration) has to be increased gradually to observe the switching when x (Co concentration) is moving away from the x_{comp}. In addition to the demonstration of the minimum Gd concentration needed to show AO-HIS, the minimum Co concentrations to sustain AO-HIS are 65, 63, and 61%, for $Gd_yTb_{1-x-y}Co_x$, $Gd_yDy_{1-x-y}Co_x$, and $Gd_yHo_{1-x-y}Co_x$, alloys, respectively. The corresponding magneto-optical
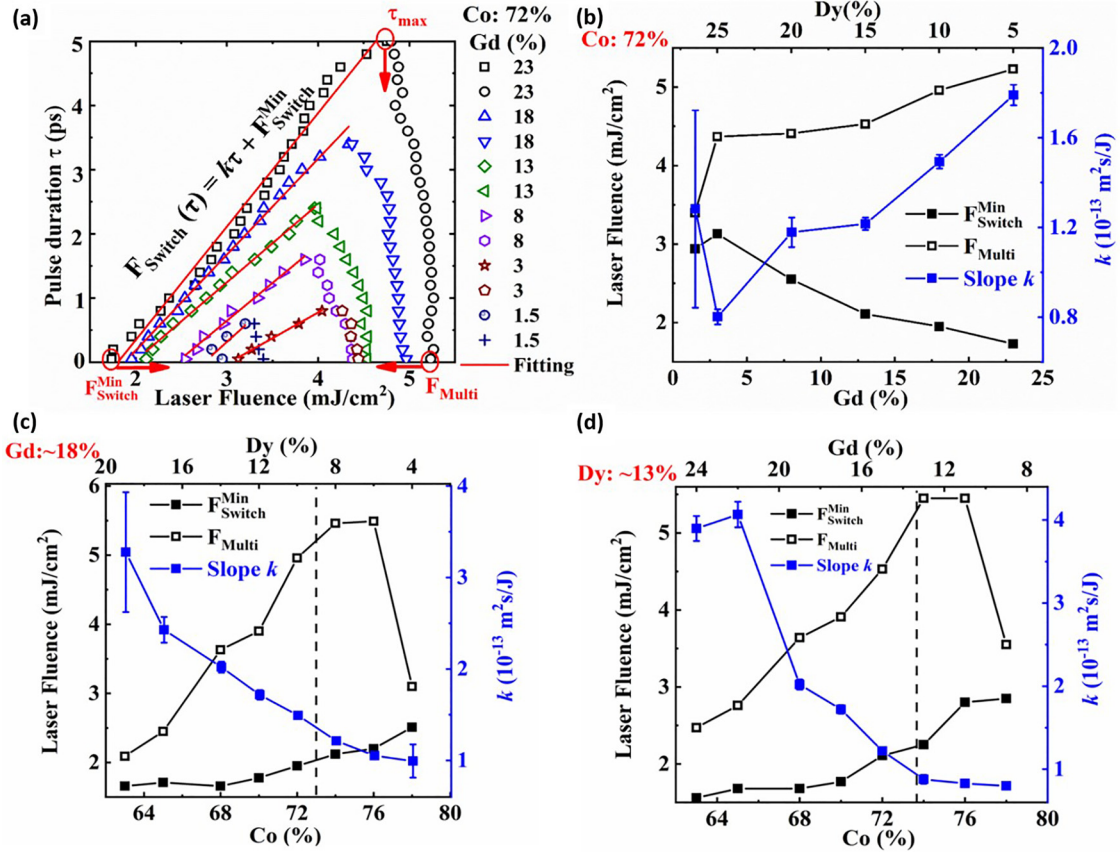
FIG. 4. Evolution of AO-HIS state diagrams for a 10-nm $Gd_yDy_{1-x-y}Co_x$ alloy sample. (a) Evolution of the magnetic-state diagrams for various Gd concentrations while the Co concentration is kept constant at $x = 72\%$, $Gd_yDy_{0.28-y}Co_{0.72}$. The parameters F_{switch}, F_{multi}, and k are extracted from (a) and Figs. S4(a) and S4(b), as a function of Gd and Co concentrations, (b) for a constant Co concentration equal to 72%, (c) for a constant Gd concentration equal to 18%, and (d) for a constant Dy concentration equal to 13%. The dashed lines in (c) and (d) correspond to the compensation point.

images after five subsequent laser pulses are shown in Fig. S3 for $Gd_{26}Tb_9Co_{65}$, $Gd_{23}Dy_{14}Co_{63}$, and $Gd_{26}Ho_{23}Co_{61}$, where one can see a clear toggle-magnetization switching. See the Appendix.

C. AO-HIS state diagrams as a function of the Gd, *RE* (Tb, Dy, or Ho), and Co concentrations

In this section, the state diagrams showing the magnetic states achieved after a single laser pulse as a function of pulse duration and fluence is investigated carefully, in order to optimize the laser parameters and the energy needed to induce magnetic switching. We start with the $Gd_{23}Dy_5Co_{72}$ sample, in which a large amount of Gd guarantees AO-HIS for a relatively large region of fluence. Figure 3(c) shows the images obtained for various laser fluences with pulse duration ranging from 50 fs to 5 ps. At first glance, the window of laser fluence allowing magnetization switching strongly depends on the pulse duration. At the shortest pulse duration $\tau = 50$ fs, this fluence window is the widest, narrowing as the pulse duration increases.

The state diagram in Fig. 3(d) is built by gathering the values of the threshold fluence (F) and pulse duration (τ) at which AO-HIS [$F_{switch}(\tau)$] and multidomain state [$F_{multi}(\tau)$]

are observed, indicated by solid black dots and open dots, respectively. Since $F_{switch}(\tau)$ and $F_{multi}(\tau)$ evolve linearly with τ, the state diagram is then defined by two (red) lines. When the laser fluence used is lower than $F_{switch}(\tau)$, the system does not respond to the laser pulse and there is no switching. This corresponds to the pink region in Fig. 3(d). When the fluence is larger than $F_{multi}(\tau)$, a multidomain state is created after the pulse, showing no AO-HIS effect. By a first approximation, F_{multi} is independent of the pulse duration, while $F_{switch}(\tau)$ increases linearly with τ. We could then use $F_{switch}(\tau) = k\tau + F_{switch}^{min}$, where F_{switch}^{min} is the minimum fluence needed to switch, experimentally obtained for the shortest pulse duration ($\tau = 50$ fs). $F_{switch}(\tau)$ and $F_{multi}(\tau)$ then define the gray triangular area showing AO-HIS. τ_{max} is therefore given by $F_{switch}(\tau_{max}) = F_{multi}(\tau_{max})$ and defines the maximum pulse duration above which AO-HIS cannot be observed, whatever the fluence. τ_{max} is then defined by three parameters: the slope k, F_{switch}^{min}, and F_{multi}.

The evolution of the state diagram as a function of the Gd concentration (as well as the concentration of Dy) when the Co concentration is fixed to 72% is shown in Fig. 4(a). All the state diagrams share a similar shape and we can still consider that $F_{switch}(\tau)$ evolves linearly with τ, whereas F_{multi} is constant. For fixed 72% Co concentration, when

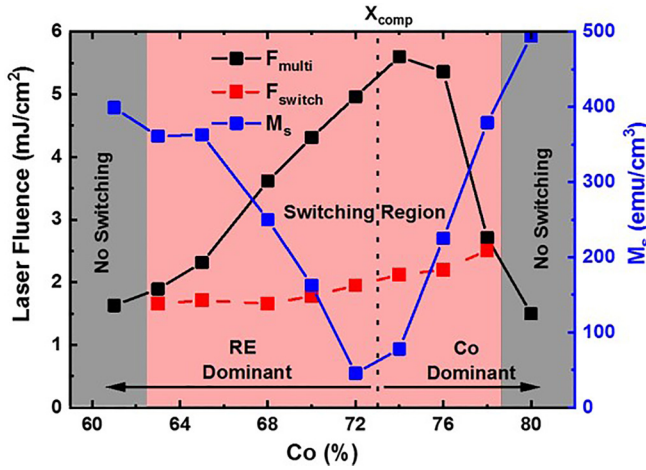FIG. 5. Evolution of F_{multi}, F_{switch}, and M_s as a function of the Co compositions for a 10-nm GdDyCo alloys, with a constant Gd concentration equal to 18%. F_{multi} and F_{switch}, are extracted from the AO-HIS experiments using a 50-fs pulse duration.

decreasing the amount of Gd, the maximum pulse duration τ_{max} and the fluence range at which AO-HIS is observed shrinks. Figure 4(b) quantitatively presents F_{switch}^{min}, F_{multi}, and k as a function of the Gd (Dy) concentrations derived from the state diagrams in Fig. 4(a). By increasing the amount of Gd, F_{switch}^{min} decreases, whereas F_{multi} and k increase, increasing τ_{max}. In Figs. S4(a) and S4(b), the evolution of the shape of state diagrams as a function of Co concentrations for constant Gd and Dy is presented. For details, please refer to the descriptions in Note 4 of Supplemental Material [21]. Based on these state diagrams, we could extract the evolution of F_{switch}^{min}, F_{multi}, and k in Figs. 4(c) and 4(d) when the concentrations of Gd and Dy are fixed, respectively. In Fig. 4(c), one can see that F_{switch}^{min} increases as the Co concentrations increases, while the slope k decreases. F_{multi} exhibits a peak close to the compensation concentration.

D. Criteria to observe AO-HIS—influence of magnetic and laser parameters

From the above results, the obvious criterion to observe AO-HIS is to have F_{switch} (τ) < F_{multi} (τ). It is true when changing the material concentrations [for example, in Figs. 4(c) and 4(d)] but also when increasing the pulse duration [Figs. 3(c) and 3(d)]. This is nicely evidenced in Fig. 5, where the evolution of F_{switch}, F_{multi}, and M_s as a function of Co concentration is shown for a fixed Gd concentration (~18%) and for a pulse duration $\tau = 50$ fs. The evolution of F_{multi} is not monotonic and depends strongly on the alloy concentration. It is a maximum at the compensation point where M_s is minimum (~50 emu/cm³), indicating an inverse relationship between M_s and F_{multi}. On the other hand, F_{switch} is varying monotonically with the Co concentration. F_{switch} does not seem to be affected by the compensation concentration, suggesting that compensation is not required and is not helping AO-HIS; however, it increases F_{multi}, which allows for the fulfillment of the $F_{switch} < F_{multi}$ criterion.

Let us now try to explain the evolution of F_{switch}^{min} (τ) and F_{multi} (τ) and consequently determine what the

requirements are to observe AO-HIS. Starting with F_{multi} (τ), we know that PMA samples tend to break into domains due to the dipolar field [26–29]. From Refs. [27] and [28], we can define a dimensionless parameter $\Delta = \frac{D_0}{t}$, where t is the sample thickness and $D_0 = \frac{\varepsilon}{E_{dem}}$ is the dipolar length. $\varepsilon = 4\sqrt{KJ}$ is the domain-wall energy per surface unit and $2\pi M_s^2$ is the demagnetizing energy per unit volume. As discussed in Refs. [27] and [28], if $\Delta = \frac{2\sqrt{K_u J_{eff}}}{\pi M_s^2 t}$ is small, the system will easily break into small domains and F_{multi} will be small, whereas if Δ is large, the system will tend to stay saturated in large domains and F_{multi} will be bigger. Consequently, F_{multi} depends on K_u, T_c, M_s, and t.

If we consider F_{switch}, most of the results described above can be understood by considering the switching as the action of the spin current generated by the demagnetization of the Gd sublattice only ($j = \frac{dM_{Gd}}{dt}$) transferring its angular momentum to the rest of the system when reaching the ordering temperature of the sample (T_c) in accord with Ref. [30]. This hypothesis is based on the results obtained in Gd-based systems [31–33] and the model developed by Remy *et al.* [34] for Gd-based spin valve structures. This agrees with the results obtained by Choi [35] suggesting the spin current generated by the Gd sublattice can interact with the transition metal when the latter is demagnetized. The F_{switch} threshold fluence will be reached when enough spin current is generated and when the spin temperature of the alloy is close enough to T_c. In those conditions, to reduce F_{switch}, one needs some combination of an increase to the Gd concentration (y_{Gd}) or a decrease to the pulse duration, T_c, or thickness of the layer, t. Consequently, F_{switch} depends on y_{Gd}, τ, T_c, and t. There are certainly two other threshold fluences which would have to be considered: the one for which the sample is demagnetized for a long period of time, also resulting in a multidomain state, and the one which will damage the sample or change its magnetic properties.

In the rest of this paper, we will check if the criteria [$F_{switch}(\tau) < F_{multi}(\tau)$] and the expected evolution of F_{switch} (τ) and F_{multi} (τ) can explain the behavior of the 300 samples involved in the present study. The layer thicknesses of the sample have been kept constant; however, all the other magnetic parameters (M_s, K_u, J_{eff}) mentioned above have been tuned by changing the alloys' concentrations and the nature of the rare earth (Tb, Dy, or Ho).

Let us consider the study presented in Fig. 5 obtained from a series of 10-nm-thick GdDyCo alloys, with a constant Gd concentration around 18% using a $\tau = 50$-fs pulse duration (i.e., t, y_{Gd} are kept constant). From the above discussion F_{switch} should only depend on T_c and F_{multi} on K_u, T_c, and M_s. The monotonical increase of F_{switch} with the Co concentration can then be understood by the fact that T_c increases with the Co concentration. The maximum value of F_{multi} at compensation can be explained by the minimum value of M_s at this point. We can then argue that the evolution of K_u and J_{eff} have little influence on F_{multi} as they only weakly vary compared to M_s and because, in the above expression of Δ, M_s is present at a power of 2, whereas K_u and J_{eff} are at a power of 1/2. From Fig. 5, we can clearly conclude that if AO-HIS cannot be observed for concentration larger than 78% and smaller than 63%, it is because for those cases F_{switch} (τ) > F_{multi} (τ).
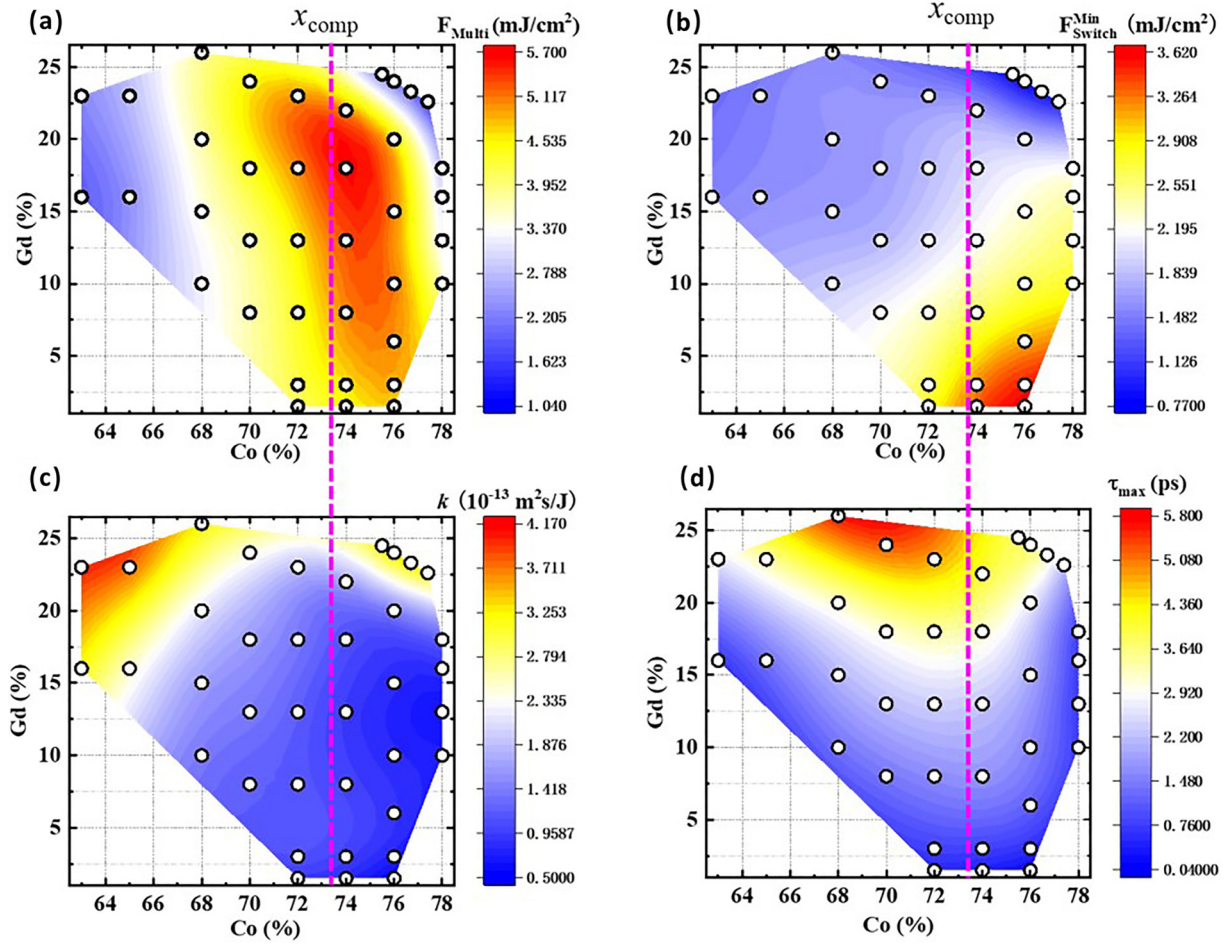
FIG. 6. Mapping of laser parameters allowing for optical magnetization switching as a function of the Gd and Co concentration for a 10-nm GdDyCo alloy. (a) The threshold laser fluence to observe multidomain state F_{multi} (b) The threshold laser fluence to observe AO-HIS F_{switch}, (c) the maximum pulse duration to observe AO-HI τ_{max}, and (d) k, the slope describing the dependence of F_{switch} on pulse duration. The dashed lines correspond to the compensation composition of the alloys. Dots indicate measured data.

Considering that the two threshold fluences can be written as follows: $F_{switch}(\tau) = k\tau + F_{switch}^{min}$ and $F_{multi}(\tau) =$ constant, Fig. 6 shows the evolution of the four parameters F_{multi}, $F_{switch}^{min} = F_{switch}$ (50 fs), k and τ_{max} as a function of the Co and Gd concentrations. From Figs. 6(a), 4(c), and 4(d) one can clearly see that F_{multi} is dominated by the value of the alloy's net magnetization, which leads to a maximum value at compensation. We mentioned that $F_{multi}(\tau)$ is almost independent of the pulse duration τ but some state diagrams show a small decrease of F_{multi} when increasing the pulse duration. This could be explained by the fact that for a given fluence, the lattice temperature is constant whatever the pulse duration; however, the electron temperature is rising to a larger value for shorter pulse duration, according to the three-temperature model [6,7,11]. If the two temperatures are very different, more dissipation will take place and consequently more energy is required to reach the threshold equilibrium temperature to allow for a multidomain state [36].

As shown in Figs. 4(c), 4(d), and 6(b), and Fig. S5, F_{switch}^{min} does increase if T_c increases but it is unclear whether it is due to the fact that T_c increases with Co concentration or because T_c(GdCo) > T_c(GdTbCo) > T_c(GdDyCo) > T_c(GdHoCo) for

a given Co and Gd concentration, as previously mentioned [37]. Unfortunately, we are unable to qualitatively determine the Curie temperature of our samples: first, because of our limited temperature range, but more importantly because the sample properties would be affected irreversibly by applying temperatures above 400 K (loss of perpendicular anisotropy). In Figs. 4(b) and 6(b), if we consider that for a given Co concentration, T_c is kept constant, F_{switch}^{min} decreases with increasing Gd due to the amount of spin current from the Gd demagnetization ($j = \frac{dM_{Gd}}{dt}$) increasing. Figure S5 demonstrates that the minimum F_{switch}^{min} is obtained for low T_c and high Gd concentration. It also explains why if the pulse duration increases, F_{switch} increases ($\frac{dM_{Gd}}{dt} \sim \frac{M_{Gd}}{\tau}$). It is amazing that even a Gd concentration as small as 1.5% is enough to switch magnetization but in this case F_{switch}^{min} is large and switching is only observed if τ is small and F_{multi} is large. It is worth addressing that the lowest Gd concentration of 1.5% is acquired when the RE-TM alloys are near the compensation point. Highlighting this issue is helpful in understanding the criteria [$F_{switch}(\tau) < F_{multi}(\tau)$] proposed in this work. For the samples near the compensation point, the value of F_{multi} is high, meaning we do not need a huge amount of Gd to reduce
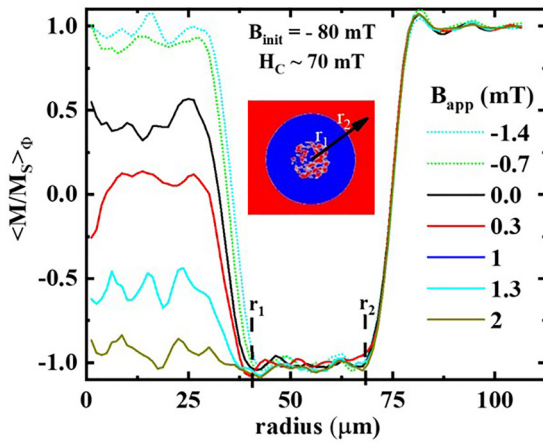
FIG. 7. Influence of applied magnetic fields on the multidomain state after a single laser pulse for a 10-nm $Gd_{18}Dy_8Co_{74}$ sample. Before the single-pulse measurements, the sample is saturated under a -80-mT field. During the laser irradiation, various external fields (-1.4, -0.7, 0, 0.3, 1, 1.3, or 2 mT) were applied. For zero applied field after a single laser pulse: multidomain structures appear for $r < r_1$, magnetization reversal for $r_1 < r < r_2$, and no magnetization change for $r > r_2$.

the value of F_{switch} for AO-HIS to be observed. On the other hand, once the sample is away from the compensation point, we can clearly see that a higher Gd concentration is necessary to observe AO-HIS [guided by the two arrows in Fig. 1(a)]. It is because more Gd leads to lower F_{switch} and this is certainly required when F_{multi} is reduced as the sample is away from the compensation.

In Figs. 6(c) and 6(d), we explicitly show the evolution of both the slope k and τ_{max} as a function of Co and Gd concentrations. The slope k is also a reflection of how easy it is to switch magnetization as one can deduce from Fig. 4(c): low values of F_{switch}^{min} give rise to large k values and vice versa. From the above discussions, our study suggests that τ_{max} is just a consequence of the crossing between F_{switch}^{min} and F_{multi}. Large τ_{max} is then obtained when both the slope of F_{switch} (τ), (k) and F_{multi}, are large.

E. Field-dependent magnetization switching and time-resolved measurements

The above results suggest that AO-HIS could be observed on much larger alloy composition and time ranges if the stray field would not break the magnetic configuration into domains, preventing the observation of AO-HIS. To prove this point, we decided to carry out two experiments. In the first one, a perpendicular magnetic field was applied to compete with the stray field. In the second one, since we expected the effect of the dipolar field to be felt at long timescales, we carried out a time-dependent measurement hoping to observe AO-HIS at short timescales and a multidomain formation at longer timescales.

As shown in Fig. 7, for a 10-nm $Gd_{18}Dy_8Co_{74}$ sample when the laser fluence $F > F_{multi}$, the multidomain structure occurs in the middle of the spot. As a result, for no applied magnetic field, three different regions are defined
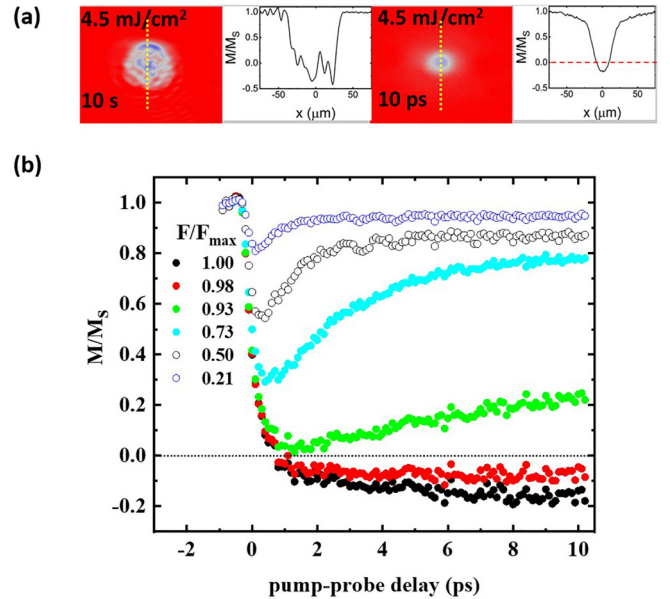

FIG. 8. Time-resolved magnetization switching dynamics on 10-nm $Gd_{13}Dy_7Co_{80}$ alloy sample. (a) Images obtained 10 s after shining the laser pulse and 10 picoseconds after shining the laser pulse. (b) Evolution of the normalized magnetization as a function of time. The sample's magnetization is reversed within less than 10 ps for proper laser fluences.

with increasing distance r from the center of the spot, i.e., multidomain ($0 < r < r_1$), switching ($r_1 < r < r_2$), and no switching ($r > r_2$). When a magnetic field much lower than the coercive field, $H_c = 70$mT, varying from $+2$ to -2 mT is applied, for $r > r_1$, no effect of the magnetic field is observed. On the contrary, we found a strong effect of magnetic field on the multidomain state at the center. The normalized magnetic contrast is around -1 when the applied field is $+2$ mT opposite to the -80-mT magnetic field applied before the laser pulse. By decreasing the external field to zero, the normalized magnetization tends to approach zero, which corresponds to the random multidomain state. Furthermore, it becomes positive, even saturated ($+1$), when a high enough negative field is applied. This evolution of the multidomain state as a function of external field suggests that the dipolar field plays a key role in the formation of the multidomain state.

The above results tend to indicate that such a stray field effect is dominant at very long timescales (quasiequilibrium state) after excitation by laser pulse. Nonetheless, it is still unclear if the magnetization can be reversed at ultrashort timescales, even in the presence of a stray field strong enough to generate multidomain states at equilibrium. We then studied the time-resolved dynamics for a 10-nm $Gd_{13}Dy_7Co_{80}$ alloy, which shows only multidomain states after single-pulse measurements [Fig. 1(a)]. The multidomain structure obtained 10 s after a single 4.5-mJ/cm^2 laser pulse is shown in Fig. 8(a). Interestingly, for the picture showing the magnetic state at 10 ps, a reversal of magnetization indicated by the negative value of the normalized magnetic contrast is observed. In Fig. 8(b), the time-resolved magnetization dynamics for a series of laser fluences demonstrate that the magnetization is

switched within less than 10 ps, although a multidomain state is observed for this sample at long timescales.

We could then conclude that in the above case and for all measured samples the limiting factor for observing AO-HIS is the multidomain formation occurring at longer timescales. One of the remaining questions and certainly one of the most important is then, "Why is gadolinium so important [38], even when present in such small quantities?" One could argue that with Gd being an *s* ion with a low spin-orbit coupling, the angular momentum generated by the Gd demagnetization is less likely to be absorbed by the lattice and thus more efficient for generating the switching [39,40]. Choi *et al.* [35] have also demonstrated that in GdFeCo alloys the spin accumulation generated by the Gd sublattice is large and is present 3 ps after the exciting laser pulse, and after the spin accumulation generated by the transition-metal sublattice at around 1 ps. The time delay before the Gd relaxation may also be an important feature leaving time for the rest of the sample to demagnetize before absorbing the angular momentum released from the Gd. Finally, considering the "Dieke diagram" presented and explained in Ref. [41] for the different rare-earth systems, it seems that for gadolinium there are no excited states available which could be reached with the energy provided by the laser pulse [42]. The latter could explain a more efficient angular momentum transfer for Gd.

From the above discussions, several possibilities could be envisioned to increase the variety of material demonstrating AO-HIS and allow the observation for larger pulse durations (i.e., increasing τ_{max}). The first idea is to study samples with in plane magnetization to avoid the generation of multidomain state-inducing stray fields. In this case, F_{multi} will not be a limiting factor. F_{switch} should then only be limited by a "real" demagnetization or the laser damaging the sample. This is what Lin *et al.* tended to demonstrate in their current work [43]. Another way of limiting the effect of F_{multi} while keeping the PMA materials is to study ultrathin samples [44]. Finally, another idea is to include a heat sink in the sample so that the heat is dissipated before the dipolar or stray fields are able to act on the magnetization to generate the dipolar field. This is what Verges *et al.* [36] showed.

III. CONCLUSIONS

In this study, the single-shot AO-HIS state diagrams for various $Gd_yRE_{1-x-y}Co_x$ (RE = Dy, Tb, Ho) alloys were systemically presented. We demonstrated that while in all those alloys, Gd is required, this can be at a concentration as low as 1.5% to still observe AO-HIS. We have determined the criteria needed to be fulfilled to observe AO-HIS by studying the evolutions of two threshold fluences: the switching fluence (F_{switch}) which leads to AO-HIS, and the multidomain fluence (F_{multi}) which leads to a multidomain state generated by the stray field present in a PMA thin film. F_{switch} is found to be given by the amount of Gd present and the Curie temperature T_c of the layer, while F_{multi} is determined by the saturated magnetization, M_s, the exchange, J_{eff}, and the anisotropy constant, K_u. Considering that $F_{switch} < F_{multi}$ is a necessary condition to observe AO-HIS, we could provide practical ways to enlarge the region of AO-HIS, including both the materials compositions and the laser parameters. From those conclusions, we could propose several types of heterostructures demonstrating AO-HIS which will be of great significance for the future of ultrafast spintronic applications.

APPENDIX: METHODS AND MATERIALS

1. Film growth

We prepared a large number of 10-nm-thick $Gd_yRE_{1-x-y}Co_x$ (RE = Dy, Tb, Ho) thin films by magnetron sputtering. Thin-film heterostructures are prepared onto a Corning 1737 float glass substrate according to the following multilayered structure: glass/Ta(5 nm)/Pt(3 nm)/$Gd_yRE_{1-x-y}Co_x$ (10 nm)/Pt(5 nm). The base pressure was $<2 \times 10^{-8}$ mbar, and a working pressure of Ar at 2×10^{-3} mbar during sputtering was maintained.

2. AO-HIS measurements

A Ti: sapphire femtosecond-laser source with a regenerative amplifier was used to generate the linearly polarized pump laser beam with a central wavelength of 800 nm (1.55 eV) and a 5-kHz repetition rate. To record the sample's magnetic state after a single ultrashort laser pulse, a Kerr microscope was used with an LED with a central wavelength around 630 nm as the light source. Pictures were taken before and after each laser shot to allow a background image correction. To ensure a well-defined initial state, the film was saturated using an external magnetic field whose exact value depends on the coercivity of the samples.

3. Pump-probe magnetization dynamics measurements

Time-resolved experiments on continuous 10-nm $Gd_{13}Dy_7Co_{80}$ alloy were conducted with a Yt fiber laser PHAROS from Light Conversion with a regenerative amplifier with a repetition rate fixed at 5 kHz. Two optical parametric amplifiers were used to tune the wavelengths of

the pump and probe beams at 800 and 650 nm with pulse durations of 100 and 178 fs, respectively. A polarizer was coupled to a half wave plate to be able to control the pump power. The spot size of the writing pulse was about 225 μm. Images have been recorded for any pump-probe delay by a charge-coupled device (CCD) (EO-5023M MONO USB CCD camera, exposure time 285.9 ms, 3.65 frames per second, accumulation of 10 images) as .tiff files. A reset magnetic field around 100 Oe is applied during the time-resolved measurements.

[1] B. Dieny, I. L. Prejbeanu, K. Garello, P. Gambardella, P. Freitas, R. Lehndorff, W. Raberg, U. Ebels, S. O. Demokritov, J. Akerman, A. Deac, P. Pirro, C. Adelmann, A. Anane, A. V. Chumak, A. Hirohata, S. Mangin, Sergio O. Valenzuela, M. Cengiz Onbaşlı, M. d'Aquino, G. Prenat, G. Finocchio, L. Lopez-Diaz, R. Chantrell, O. Chubykalo-Fesenko, and P. Bortolotti, Opportunities and challenges for spintronics in the microelectronics industry, Nat. Electronics. **3**, 446 (2020).

[2] K. C. Chun, H. Zhao, J. D. Harms, T. Kim, J. Wang, and C. H. Kim, A Scaling roadmap and performance evaluation of in-plane and perpendicular MTJ based STT-MRAMs for high-density cache memory, IEEE J. Solid-State Circuits. **48**, 598 (2013).

[3] D. Sander, S. O. Valenzuela, D. Makarov, C. H. Marrows, E. E. Fullerton, P. Fischer, J. McCord, P. Vavassori, S. Mangin, P. Pirro, B. Hillebrands, A. D. Kent, T. Jungwirth, O. Gutfleisch, C. G. Kim, and A. Berger, The 2017 Magnetism Roadmap, J. Phys. D: Appl Phys. **50**, 363001 (2017).

[4] Y. S. Liu, H. Y. Cheng, Y. Xu, P. Vallobra, S. Eimer, X. Q. Zhang, X. J. Wu, T. X. Nie, and W. S. Zhao, Separation of emission mechanisms in spintronic terahertz emitters, Phys. Rev. B **104**, 064419 (2021).

[5] T. Seifert, S. Jaiswal, U. Martens, J. Hannegan, L. Braun, P. Maldonado, F. Freimuth, A. Kronenberg, J. Henrizi, and I. Radu, Efficient metallic spintronic emitters of ultrabroadband terahertz radiation, Nat. Photonics. **10**, 483 (2016).

[6] F. Jakobs, T. A. Ostler, C.-H. Lambert, Y. Yang, S. Salahuddin, R. B. Wilson, J. Gorchon, J. Bokor, and U. Atxitia, Unifying femtosecond and picosecond single-pulse magnetic switching in Gd-Fe-Co, Phys. Rev. B **103**, 104422 (2021).

[7] I. Radu, K. Vahaplar, C. Stamm, T. Kachel, N. Pontius, H. A. Dürr, T. A. Ostler, J. Barker, R. F. L. Evans, R. W. Chantrell, A. Tsukamoto, A. Itoh, A. Kirilyuk, T. Rasing, and A. V. Kimel, Transient ferromagnetic-like state mediating ultrafast reversal of antiferromagnetically coupled spins, Nature (London). **472**, 205 (2011).

[8] Y. Xu, M. Deb, G. Malinowski, M. Hehn, W. Zhao, and S. Mangin, Ultrafast magnetization manipulation using single femtosecond light and hot-electron pulses, Adv. Mater. **29**, 1703474 (2017).

[9] C. S. Davies, T. Janssen, J. H. Mentink, A. Tsukamoto, A. V. Kimel, A. F. G. van der Meer, A. Stupakiewicz, and A. Kirilyuk, Pathways for single-shot all-optical switching of magnetization in ferrimagnets, Phys. Rev. Appl. **13**, 024064 (2020).

[10] Y. Xu, M. Hehn, W. Zhao, X. Lin, G. Malinowski, and S. Mangin, From single to multiple pulse all-optical switching in GdFeCo thin films, Phys. Rev. B **100**, 064424 (2019).

[11] Y. Xu and S. Mangin, Magnetization manipulation using ultrashort light pulses, J. Magn. Magn. Mater. **564**, 170169 (2022).

[12] M. L. M. Lalieu, M. J. G. Peeters, S. R. R. Haenen, R. Lavrijsen, and B. Koopmans, Deterministic all-optical switching of synthetic ferrimagnets using single femtosecond laser pulses, Phys. Rev. B **96**, 220411(R) (2017).

[13] L. Avilés-Félix, A. Olivier, G. Li, C. S. Davies, L. Álvaro-Gómez, M. Rubio-Roy, S. Auffret, A. Kirilyuk, A. V. Kimel, Th. Rasing, L. D. Buda-Prejbeanu, R. C. Sousa, B. Dieny, and I. L. Prejbeanu, Single-shot all-optical switching of magnetization in Tb/Co multilayer-based electrodes, Sci. Rep. **10**, 5211 (2020).

[14] C. Banerjee, N. Teichert, K. E. Siewierska, Z. Gercsi, G. Y. P. Atcheson, P. Stamenov, K. Rode, J. M. D. Coey, and J. Besbas, Single pulse all-optical toggle switching of magnetization without gadolinium in the ferrimagnet Mn$_2$Ru$_x$Ga, Nat. Commun. **11**, 4444 (2020).

[15] Y. Peng, D. Salomoni, G. Malinowski, W. Zhang, J. Hohlfeld, L. D. Buda-Prejbeanu, J. Gorchon, M. Vergès, J. X. Lin, R. C. Sousa, I. L. Prejbeanu, S. Mangin, and M. Hehn, In-plane reorientation induced single laser pulse magnetization reversal, Nat. Commun. **14**, 5000 (2023).

[16] J. Q. Wei, B. Y. Zhang, M. Hehn, W. Zhang, G. Malinowski, Y. Xu, W. S. Zhao, and S. Mangin, All-optical helicity-independent switching state diagram in GdFeCo alloys, Phys. Rev. Appl. **15**, 054065 (2021).

[17] M. Beens, M. L. M. Lalieu, A. J. M. Deenen, R. A. Duine, and B. Koopmans, Comparing all-optical switching in synthetic-ferrimagnetic multilayers and alloys, Phys. Rev. B **100**, 220409(R) (2019).

[18] C. S. Davies, J. H. Mentink, A. V. Kimel, Th. Rasing, and A. Kirilyuk, Helicity-independent all-optical switching of magnetization in ferrimagnetic alloys, J. Magn. Magn. Mater. **563**, 169851 (2022).

[19] R. Moreno, T. A. Ostler, R. W. Chantrell, and O. Chubykalo-Fesenko, Conditions for thermally induced all-optical switching in ferrimagnetic alloys: Modeling of TbCo, Phys. Rev. B **96**, 014409 (2017).

[20] J. Gorchon, R. B. Wilson, Y. Yang, A. Pattabi, J. Y. Chen, L. He, J. P. Wang, M. Li, and J. Bokor, Role of electron and phonon temperatures in the helicity-independent all-optical switching of GdFeCo, Phys. Rev. B **94**, 184406 (2016).

[21] See Supplemental Material at http://link.aps.org/supplemental/10.1103/PhysRevB.109.094412 for the mapping of the magnetic states after one single ultrashort laser pulse; magnetization-toggle switching in Gd$_y$RE$_{1-x-y}$Co$_x$ samples; evolution of the shape of state diagrams; summary of threshold fluence to observe switching and multidomains for different Gd*RE*Co alloys.

[22] P. Hansen, S. Klahn, C. Clausen, G. Much, and K. Witter, Magnetic and magneto-optical properties of rare-earth transition-metal alloys containing Dy, Ho, Fe, Co, J. Appl. Phys. **69**, 3194 (1991).

[23] P. Hansen, C. Clausen, G. Much, M. Rosenkranz, and K. Witter, Magnetic and magneto-optical properties of rare-earth

transition-metal alloys containing Gd, Tb, Fe, Co, J. Appl. Phys. **66**, 756 (1989).

[24] A. Ceballos, A. Pattabi, A. El-Ghazaly, S. Ruta, C. P. Simon, R. F. L. Evans, T. Ostler, R. W. Chantrell, E. Kennedy, M. Scott, J. Bokor, and F. Hellman, Role of element-specific damping in ultrafast, helicity-independent, all-optical switching dynamics in amorphous (Gd,Tb)Co thin films, Phys. Rev. B **103**, 024438 (2021).

[25] C. D. Stanciu, A. V. Kimel, F. Hansteen, A. Tsukamoto, A. Itoh, A. Kirilyuk, and Th. Rasing, Ultrafast spin dynamics across compensation points in ferrimagnetic GdFeCo: The role of angular momentum compensation, Phys. Rev. B **73**, 220402(R) (2006).

[26] C. Kooy and U. Enz, Experimental and theoretical study of the domain configuration in thin layers of BaFeO, Philips Res. Rep. **15**, 7 (1960).

[27] O. Hellwig, A. Berger, J. B. Kortright, and E. E. Fullerton, Domain structure and magnetization reversal of antiferromagnetically coupled perpendicular anisotropy films, J. Magn. Magn. Mater. **319**, 13 (2007).

[28] M. Salah El Hadri, M. Hehn, P. Pirro, C-H. Lambert, G. Malinowski, E. E. Fullerton, and S. Mangin, Domain size criterion for the observation of all-optical helicity-dependent switching in magnetic thin films, Phys. Rev. B **94**, 064419 (2016).

[29] A. Westover, K. Chesnel, K. Hatch, P. Salter, and O. Hellwig, Enhancement of magnetic domain topologies in Co/Pt thin films by fine tuning the magnetic field path throughout the hysteresis loop, J. Magn. Magn. Mater. **399**, 164 (2016).

[30] M. Beens, K. A. de Mare, R. A. Duine, and B. Koopmans, Spin-polarized hot electron transport versus spin pumping mediated by local heating, J. Phys.: Condens. Matter **35**, 035803 (2022).

[31] Q. Remy, J. Igarashi, S. Iihama, G. Malinowski, M. Hehn, J. Gorchon, J. Hohlfeld, S. Fukami, H. Ohno, and S. Mangin, Energy efficient control of ultrafast spin current to induce single femtosecond pulse switching of a ferromagnet, Adv. Sci. **7**, 2001996 (2020).

[32] S. Iihama, Y. Xu, M. Deb, G. Malinowski, M. Hehn, J. Gorchon, E. E. Fullerton, and S. Mangin, Single-shot multi-level all-optical magnetization switching mediated by spin transport, Adv. Mater. **30**, 1804004 (2018).

[33] J. Igarashi, W. Zhang, Q. Remy1, E. Díaz, J. X. Lin, J. Hohlfeld, M. Hehn, S. Mangin, J. Gorchon, and G. Malinowski, Optically induced ultrafast magnetization switching in ferromagnetic spin valves, Nat. Mater. **22**, 725 (2023).

[34] Q. Remy, J. Hohlfeld, M. Vergès, Y. Le Guen, J. Gorchon, G. Malinowski, S. Mangin, and M. Hehn, Accelerating ultrafast magnetization reversal by non-local spin transfer, Nat. Commun. **14**, 445 (2023).

[35] G. M. Choi and B. C. Min, Laser-driven spin generation in the conduction bands of ferrimagnetic metals, Phys. Rev. B **97**, 014410 (2018).

[36] M. Verges, W. Zhang, Q. Remy, Y. Le-Guen, J. Gorchon, G. Malinowski, S. Mangin, M. Hehn, and J. Hohlfeld, Extending the scope and understanding of all-optical magnetization switching in Gd-based alloys by controlling the underlying temperature transients, Phys. Rev. Appl. (to be published).

[37] J. Stohr and H. C. Siegmann, *Magnetism: From Fundamentals to Nanoscale Dynamics* (Higher Education Press, 2012).

[38] T. Lichtenberg, Y. L. W. van Hees, M. Beens, C. J. Levels, R. Lavrijsen, R. A. Duine, and B. Koopmans, Probing laser-induced spin-current generation in synthetic ferrimagnets using spin waves, Phys. Rev. B **106**, 094436 (2022).

[39] W. Zhang, J. X. Lin, T. X. Huang, G. Malinowski, M. Hehn, Y. Xu, S. Mangin, and W. S. Zhao, Role of spin-lattice coupling in ultrafast demagnetization and all optical helicity-independent single-shot switching in $Gd_{1-x-y}Tb_yCo_x$ alloys, Phys. Rev. B **105**, 054410 (2022).

[40] N. Bergeard, V. López-Flores, V. Halte, M. Hehn, C. Stamm, N. Pontius, E. Beaurepaire, and C. Boeglin, Ultrafast angular momentum transfer in multisublattice ferrimagnets, Nat. Commun. **5**, 3466 (2014).

[41] I. T. Sorokina, *Solid-State Mid-Infrared Laser Sources* (Springer, 2003).

[42] M. Coey (private communication).

[43] J. X. Lin, M. Hehn, T. Hauet, Y. Peng, J. Igarashi, Y. Le Guen, Q. Remy, J. Gorchon, G. Malinowski, S. Mangin, and J. Hohlfeld, Single laser pulse induced magnetization switching in in-plane magnetized GdCo alloys, Phys. Rev. B **108**, L220403 (2023).

[44] D. P. G. Nyoma, M. Hehn, G. Malinowski, J. Ghanbaja, J. Hohlfeld, J. orchon, S. Mangin, and F. Montaigne, Gd doping at the Co/Pt interfaces to induce ultrafast all-optical switching, ACS Appl. Electron. Mater **6**, 1122 (2024).